Title

Stability of rare-earth-doped spherical yttria-stabilized zirconia synthesized by ultrasonic spray pyrolysis

Journal

Journal of the American Ceramic Society, 100(10)

ISSN

0002-7820

Authors

Nafsin, Nazia
Li, Hui
Leib, Elisabeth W
et al.

Publication Date

2017-10-01

DOI

10.1111/jace.14971

Peer reviewed

Received: 21 November 2016 | Accepted: 4 May 2017

DOI: 10.1111/jace.14971

ORIGINAL ARTICLE

Journal of the American Ceramic Society

Stability of rare-earth-doped spherical yttria-stabilized zirconia synthesized by ultrasonic spray pyrolysis

Nazia Nafsin[1] | Hui Li[1] | Elisabeth W. Leib[2] | Tobias Vossmeyer[2] | Pieter Stroeve[3] | Ricardo H. R. Castro[1]

[1]Department of Materials Science and Engineering & NEAT ORU, University of California-Davis, Davis, California

[2]Institute of Physical Chemistry, University of Hamburg, Hamburg, Germany

[3]Department of Chemical Engineering, University of California-Davis, Davis, California

Correspondence
Ricardo H. R. Castro, Department of Materials Science and Engineering & NEAT ORU, University of California-Davis, Davis, CA
Email: rhrcastro@ucdavis.edu

Funding information
Nuclear Energy University Programs, Grant/Award Number: DE-NE0000704; Deutsche Forschungsgemeinschaft, Grant/Award Number: SFB 986

Abstract

Phase stability is one of the crucial requirements for any material that can be used at elevated temperature applications such as thermal barrier coating (TBC). The most traditional TBC material, partially stabilized zirconia, limits the operating temperature due to its phase transformation. Conversely, the low thermal conductivity of fully stabilized zirconia (YSZ) may enable effective reduction in the surface temperature on the coated component, while avoiding deleterious phase transitions, although still being subjected to sintering and grain growth. It has been reported that addition of rare-earths as dopants to YSZ can significantly increase resistance to grain growth at high temperature. Keeping this under consideration, this work investigates the role of rare-earths (lanthanum and gadolinium) in increasing thermal stability of YSZ microspheres, the building blocks for high-temperature photonics for reflective TBC. The spheres were produced by ultrasonic spray pyrolysis, and the doping led to significant improvement of stability by significant inhibition of grain growth. While the individual dopants showed significant growth and sintering inhibition up to 900°C, co-doping with 4% (in mol) of each (Gd and La) led to coarsening resistance up to 1000°C for 3 hours, when particles retained reasonable spherical features with nanometric crystallite sizes.

KEYWORDS

coarsening, spray pyrolysis, zirconia: yttria stabilized

1 | INTRODUCTION

Among the widespread applications of zirconia ceramics, its use as a thermal barrier coating (TBC) has been intensively investigated in the past decades. TBCs are generally applied on metallic surfaces of gas turbine or aeroengine parts, operating at elevated temperatures, as a form of exhaust heat management. Several developments of ceramic TBC have been made for turbine parts due to the limited temperature stability of traditional turbine materials.[1,2] The purpose of TBC is to provide a low thermal conductivity barrier to heat transfer, from the hot gas in the engine to the surface of the coated alloy component, whether in the combustor or the turbine.[3,4] The TBC allows to increase the gas temperature of the turbine, and thereby the engine efficiency, without increasing the surface temperature of the alloy. Moreover, it also protects from rapid thermal transients to occur due to flame out and simplifies the turbine blade design by minimizing thermal distortions of the blade.[1,2] The choice of proper materials as a TBC for turbine engine can extend its life by decreasing the surface temperature of that component. Two of the most important characteristics of an effective TBC are low thermal diffusivity and phase

stability during thermal cycling between room temperature and operation temperature.[5,6]

According to Miller et al., the first use of TBCs in manned flight was in 1960s.[5] As a TBC, calcia-stabilized zirconia was used on the exhaust nozzle of the X-15 manned rocket plane.[5] Later, several ceramic coatings such as Al_2O_3,[7,8] mullite,[6,9] CaO/MgO+ZrO_2,[5] YSZ,[10-13] CeO_2+YSZ,[14] $La_2Zr_2O_7$,[15,16] etc. have been tested as TBC materials. However, their limitations as a coating material under extreme operating conditions which subjects to severe mechanical, chemical, and thermal stresses continue to lead researchers to look for better solutions. For instance, partially stabilized YSZ has limited operational temperature (<1200°C) for long-term application. Over 1200°C, phase transformations from tetragonal to tetragonal and cubic (t+c) and then during cooling again to monoclinic (m) occur, giving rise to the formation of cracks in the coating.[15] In case of mullite, above 1000°C, the thermal cycling life of coating is much shorter than that of partially stabilized YSZ.[15] Moreover, mullite coating crystallizes at 750°C-1000°C, accompanied by a volume contraction, causing cracking, and de-bonding.[17] The addition of CeO_2 in YSZ can affect the coating hardness and stoichiometry due to the vaporization of CeO_2, reduction of CeO_2 into Ce_2O_3 and accelerated sintering rate of the coating.[18] Even $La_2Zr_2O_7$ has shorter thermal cycling life than partially stabilized YSZ coating which might be explained by its relatively low thermal expansion coefficient and toughness.[19]

Recent developments in high-temperature photonic structures (HTPS) have allowed the increased radiation reflectance by means of nanolayered coatings (without significant sintering). This can decrease the surface temperature of gas turbine blades by up to 180°C, which could lead to a significant improvement of blade lifetime.[20] Addition of rare earth (RE) dopant in YSZ can enhance the thermal stability and reduce thermal conductivity of TBC by 50%, as reported by Zhuand Miller,[21] from 1.85 to 1.90 W m^{-1} K^{-1} (4.6 mol% YSZ) to 0.85 W m^{-1} K^{-1}after 20 hours high-temperature testing (for ZrO_2-(4-6 mol%) (Y. Nd. Yb)$_2O_3$ oxide cluster coatings). The reduction in thermal conductivity is because of the presence of 5-100 nm defect clusters distributed throughout the coating matrix, which limit the mean free path of both phonons and photons.

Ideally, a perfect TBC material with photonic structure must have spherical and highly monodispersed particles, with sizes of 3 μm (so that it can reflect incoming IR) and have thermal stability at elevated operating temperature.[22,23]Several synthesis techniques have been developed for spherical YSZ or zirconia based ceramic oxides such as polymer induced colloid aggregation,[24-27] sol gel,[22,28-32] and spray pyrolysis.[33-37] Ultrasonic spray pyrolysis (USP) was used in the present work because it is a continuous, low cost, and single-step method for the preparation of fine, spherical particles, with a narrow size distribution, highly crystalline, and good stoichiometry, chemically homogeneous, and is suitable for multicomponent powders (allowing proper doping for coarsening control, for instance).[33,38] The USP technique is based on the assumption that one droplet forms one product particle (sphere),[39] i.e., the precursor solution is atomized into liquid droplets that are carried by gas into a hot zone where they are rapidly heated and decomposed to form spherical oxide particles.[39,40]

The purpose of this work is to study the applicability of USP for the synthesis of spherical particles suitable for TBC. Considering the requirements for this application, this work focuses on fully stabilized 12% (in mol) YSZ spherical particles to avoid phase transformations since, at this composition, YSZ remains in cubic phase until its melting temperature.[41] Moreover, since YSZ may suffer grain growth at high temperatures, the suitability of the USP to dope YSZ with RE was also examined.[42] RE elements are expected to segregate to the grain boundary of ceramics, lowering interface energies, hypothetically allowing robust resistance to coarsening even at extremely high temperatures.[42,43] To understand effect of dopant cation radius on growth resistance in YSZ, two different dopants, lanthanum (La, ionic radius 103 pm) and gadolinium (Gd, ionic radius 94 pm), were selected and used under different concentrations. Given the initial positive results with the individual dopants on the thermal stability, co-doping was also tested and revealed a further increase in thermal stability, with the spheres holding shape and crystallite sizes in the nanoscale up to 1000°C for at least 3 hours.

2 | EXPERIMENTAL PROCEDURE

USP was used to synthesize YSZ based sphere-like particles. As precursors, zirconium oxynitrate hydrate [$ZrO(NO_3)_3.xH_2O$] (Aldrich, 99%, St. Louis, MO), yttrium nitrate hexahydrate [$Y(NO_3)_3.6H_2O$] (Aldrich, 99.999%, St. Louis, MO) were dissolved in water (0.1 mol L^{-1} solution) and sprayed through the reactor tube (GSL-1700X, MTI Corporation, KJ Group, California, USA) using two atomizers (1.7 MHz each) with a carrier airflow of 9 l min^{-1}. For the RE doping, Gadolinium nitrate hexahydrate [$Gd(NO_3)_3.6H_2O$] (Aldrich, 99.999%, St. Louis, MO) and Lanthanum nitrate hexahydrate [$La(NO_3)_3.6H_2O$] (Aldrich, 99.999%, St. Louis, MO) were also added into the salt solution. The liquid droplets created by the atomizers were transformed into oxide particles after passing through the hot zone of a tube furnace. Synthesis temperatures were 1100°C or 1300°C. Temperatures were enough to cause complete decomposition of the precursors, as tested using thermogravimetry (see Figure S1). Obtained oxide particles were passed through an electrostatic precipitator (1.5 kV)

for collection. The powders were then separated by washing the electrostatic precipitator with ethanol and evaporating the solvent. Generally, oxides synthesized by USP process do not need any further calcination, but for the calorimetric measurement, powders were calcined at 500°C for 2 hours to remove any residual carbon contaminants.

Chemical compositions were confirmed by X-ray Fluorescence (XRF) spectroscopy (Rigaku, Supermini200 Sequential WD-XRF, Pd Target, 50 kV, 4 mA, Tokyo, Japan). The phase purity was ensured using X-ray diffraction (XRD) technique (Bruker AXS Inc., Madison, WI, model D8 Advance; CuKα Radiation λ=1.5418 Å under 40 kV and 40 mA) and crystallite size of those calcined particles determined by whole profile fitting of the XRD patterns by using JADE 6.1(MDI) software.

In order to understand the effect of individual dopants in the coarsening behavior of the spherical particles, differential scanning calorimeter (DSC, Setsys 1750 Evolution, Setaram, France) was used to heat up the powders up to 1100°C in an Ar atmosphere at a rate of 20°C min^{-1} and held at that temperature for 30 minutes. This caused coarsening of the grains which had their respective heat evolution monitored by the calorimeter for further correlation with the microstructure.[44,45]

The direct effect of dopants in stabilizing spherical particles was evaluated by annealing them in air at several different temperatures (700-1200°C) for 3 hours in a reactor furnace (GSL 1700X, MTI Corporation, KJ Group, California, USA). As co-doped YSZ spheres were synthesized at higher temperature, the annealing temperatures were stretched to 1200°C. Microstructures of all the YSZ samples were characterized by Scanning Electron Microscopy (SEM; FEI Company, FEI 430NanoSEM, Hillsboro, Oregon) and the grain sizes were measured by ImageJ software by linear intersecting method. Transmission electron microscopy, (TEM) JEOL 2100 with STEM Annular Dark Field (ADF) detector (Voltage 200 kV, emission current 137 μA), was also used to see the particle morphology.

3 | RESULTS AND DISCUSSION

USP was performed at 1100°C to obtain YSZ and YSZ doped with 1 or 2% (in mol) La and doped with 2% Gd. Figure 1 shows SEM images of the highly isotropic spheres obtained from the method, independent on the composition. While individual particles could be found, small aggregates are commonly observed. However, the aggregation seems to be a result of the sample preparation for the SEM rather than sintering since one can also observe the apparent "necking" features in some particles with the SEM stub itself, suggesting it is not a sintering related neck, but probably due to the gold coating that was deposited prior to SEM imaging. XRD patterns for all samples shown in Figure 2 confirm that all reflection peaks match the characteristic ones for cubic zirconia. No second phases were observed even for the RE-doped

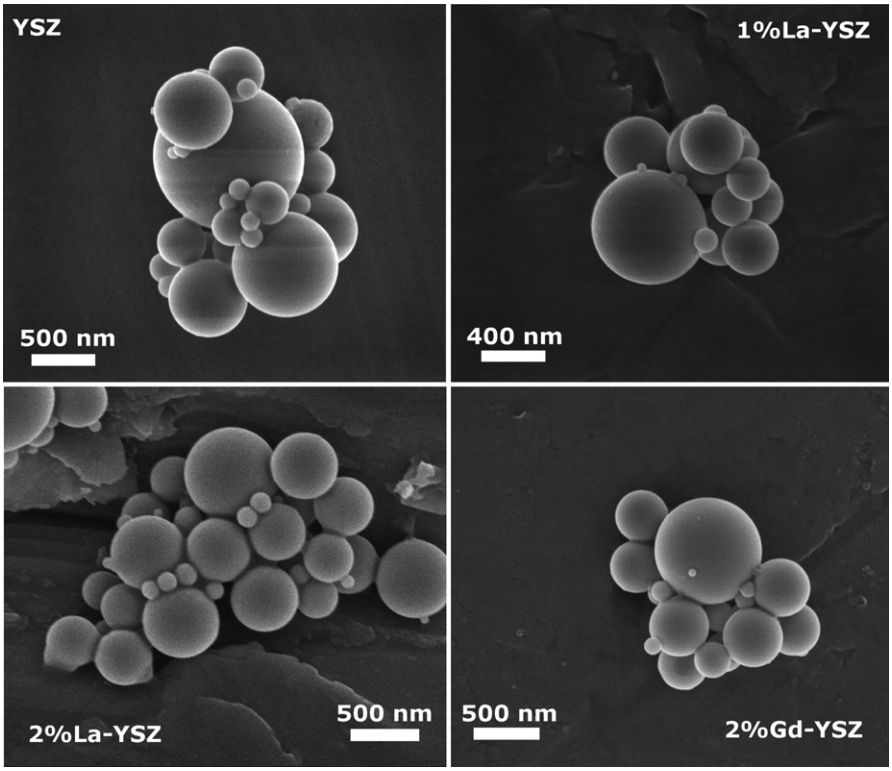

FIGURE 1 SEM micrographs of YSZ and RE-doped YSZ spheres prepared by USP and further calcined at 500°C for 2 hours

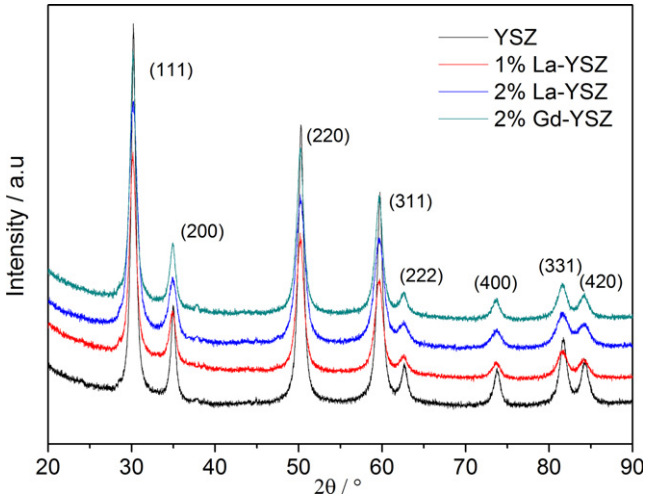

FIGURE 2 XRD patterns of RE-doped and RE-free YSZ spheres after calcination at 500°C. YSZ pattern is the bottom one, followed by 1% La, 2% La and finally 2% Gd at the top

TABLE 1 Crystallite size and sphere size of RE-free and RE-doped YSZ prepared by USP at 1100°C or 1300°C and after calcination

Sample	Crystallite size (XRD)/nm	Particle size (SEM)/nm
USP at 1100°C		
12YSZ	13.4±0.7	443±207
1% La YSZ	9.0±0.4	347±184
2% La YSZ	7.3±0.3	330±176
2% Gd YSZ	9.9±0.4	370±193
USP at 1300°C		
8% Gd YSZ	15.6±1.4	502±289 (nonspherical)
8% La YSZ	9.1±1.1	462±180 (second phase)
1%Gd-1%La YSZ	17.4±0.9	298±275
2%Gd-2%La YSZ	12.6±0.5	236±166
4%Gd-4%La YSZ	8.0±0.4	296±176

samples. From the peak positions, one cannot observe significant changes in lattice parameters, indicating that the RE dopants (Gd/La) are likely not forming solid solution (which would lead to significant lattice expansion given the radius mismatch with the ions from the YSZ crystal). This suggests the RE dopants are segregated to the grain boundaries, as previously reported to occur in La- and Gd-doped YSZ prepared by other methods.[42,46] The XRD peaks are, however, significantly broad, suggesting nanocrystalline grain sizes. Crystallite sizes calculated with whole profile fitting show that the RE-free YSZ has 13.4 nm grains, while the RE-doped YSZ show systematically smaller crystallites (see Table 1). This fact is again consistent with the segregation of RE to the interfaces, that is expected to lower interfacial energies and hinder coarsening, as reported previously.[42,43] Interestingly, one observes that not only the crystallite size is decreased, but also the size of the spheres themselves. Table 1 lists the sizes measured from multiple SEM images (size distributions can be found in the Supplemental Information, Figure S2).

The RE dopants are not expected to affect the size of the liquid droplets, and because of their small concentration and compatible chemistry (as compared to Y and Zr precursors), the surface tension of the liquid should not be significantly affected. This suggests that RE dopants are affecting the crystallization of the spheres during USP. We speculate the RE dopants are segregating to the grain boundaries, energetically stabilizing them and promoting their formation. This would result in more shrank particles as schematically shown in Figure 3.

STEM dark field image in Figure 3 reveals the morphology of RE-free and 2% La YSZ calcined particle (representative). The particles are highly porous, as confirmed by the contrasts which suggest a sponge-like form. The pores are very small although, with less than 10 nm. Porous spheres produced by USP have been predicted in the literature[35,47] but rarely demonstrated. This feature is quite beneficial for application in TBC, given that the presence of pores will further decrease thermal conductivity due to the low thermal conductivity of air.[48]

The grain stabilization demonstrated in Table 1 for the as-synthesized particles suggest an increased thermal stability. To assess this, direct calorimetric experiments in DSC were performed. Figure 4 shows the DSC curves for all compositions resulting from a constant heating rate up to 1100°C. Clear exothermic peaks are observed for all samples and attributed to coarsening (and possible collapsing) of the spherical structures. There is postponement of the exothermic peak onset as a function of RE doping. From YSZ, the peak starts at about 650°C, which is postponed to 700°C for 1% La (and 2% Gd) and to 800°C for 2 mol% La. This means increased but still limited thermal stability of the spheres.

After DSC, all samples were analyzed in terms of XRD and SEM to quantify the effect of heating (1100°C) on phase purity, crystallite size and particle size. The XRD patterns are presented in Figure S3. The samples remained in the fluorite structure, without the presence of second phases. It was found that after 1100°C the crystallites have grown to an extent that is beyond the measurement limit (>100 nm) of XRD. So SEM was performed to measure the grain size of the samples after DSC. For RE-doped YSZ, decrease in crystallite size was found as compared to YSZ and depends on the type and concentration of dopant, as listed in Table 2. However, it is important to note that these are grain sizes instead of particle size, because at

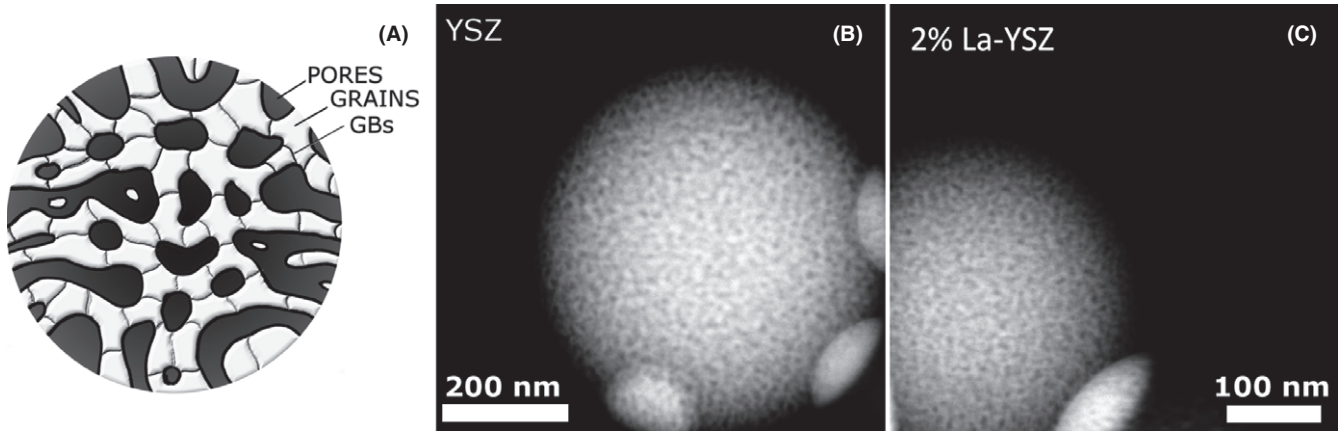

FIGURE 3 A, Schematics of YSZ spheres where grain boundaries (GBs) are responsible for structural strength. RE dopants stabilize GBs by lowering their energies. B and C, STEM micrograph of YSZ and 2% La-doped YSZ spheres after calcination at 500°C. The particle (sphere) sizes are 553 nm and 300 nm, respectively

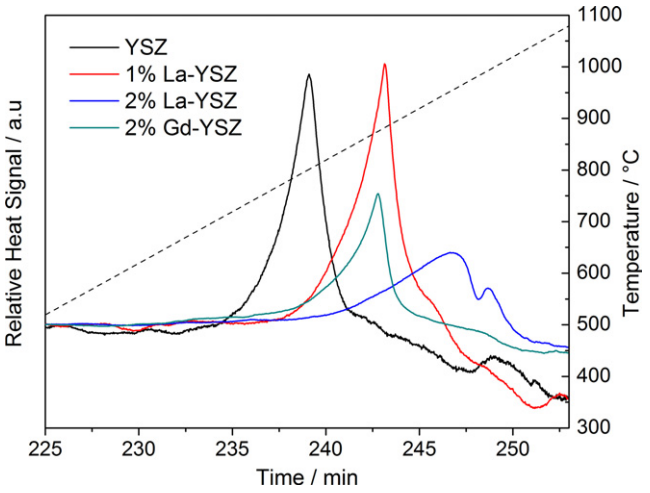

FIGURE 4 Differential scanning calorimetry heat signals of YSZ and RE-doped YSZ. Peaks are exothermic. YSZ curve is the peak at the most left, followed by 1% La and 2% Gd (second from left high and low peak, respectively) and the smallest peak to the right is for 2% La

TABLE 2 Grain size and enthalpy change of RE-free and RE-doped YSZ after DSC

Sample	Enthalpy change (Exo.)/J.g^{-1}	Grain size (SEM)/nm
12YSZ	30.45±0.56	3634±1416
1% La YSZ	28.51±0.25	2466±1334
2% La YSZ	20.06±0.16	1094±517
2% Gd YSZ	29.62±0.46	1802±668

1100°C the particles grow too much so that the spherical shapes are compromised, as exemplified in Figure S4.

The integral of the heat signals are shown in Table 2. The exothermic heat related to the grain growth was significantly influenced by the dopant ionic radius as well as their concentration. The heat signal reduced from 30.45 J g^{-1} (for YSZ) to 20.06 J g^{-1} (for 2% La YSZ). Since the ionic radius of Gd (94 pm) is smaller than La (103 pm), for the same concentration of dopant, the heat effect for grain growth by 2% La addition is much smaller than that of 2% Gd YSZ (29.62 J g^{-1}). Similarly, for the same dopant (La), their concentration at the boundaries also significantly affects the grain growth energy (from 28.51 J g^{-1} for 1% La to 20.06 J g^{-1} for 2% La). The apparent dependency of the growth heat on the ionic radius of the dopant can be related to the amount of dopant segregated to the interfaces. That is, the grain-boundary energy is a function of the excess of dopants at the grain boundaries (as will be discussed later), and the larger the difference between the ionic radius of the host material and the dopant, the stronger the tendency to segregate.[23,24] The reduction in the energy of coarsening is consistent with previous studies appointing that RE segregates to the grain boundaries and reduce local energies.[42,43] For instance, 2% La was observed to decrease the grain-boundary energy of YSZ from 1.01 J m^{-2} to 0.54 J m^{-2}.[42] Similarly, 2% Gd has been shown to decrease the grain-boundary energy to 0.75 J m^{-2}.[43] The decrease in grain-boundary energy caused by the RE doping thus decreases the excess energies, which are the main driving forces for the growth and eventual collapsing of the YSZ spheres.

In order to evaluate the microstructure evolution and thermal stability of the as-synthesized spheres, the calcined RE-free and RE-doped YSZ were annealed in air at 700°C, 800°C, 900°C, and 1000°C for 3 hours and their phase stability, crystallite size, and shape were analyzed using XRD and SEM. Figure 5 shows the XRD patterns of YSZ spheres after annealing. The patterns show no trace of second phase formation during annealing. The peaks match with the cubic

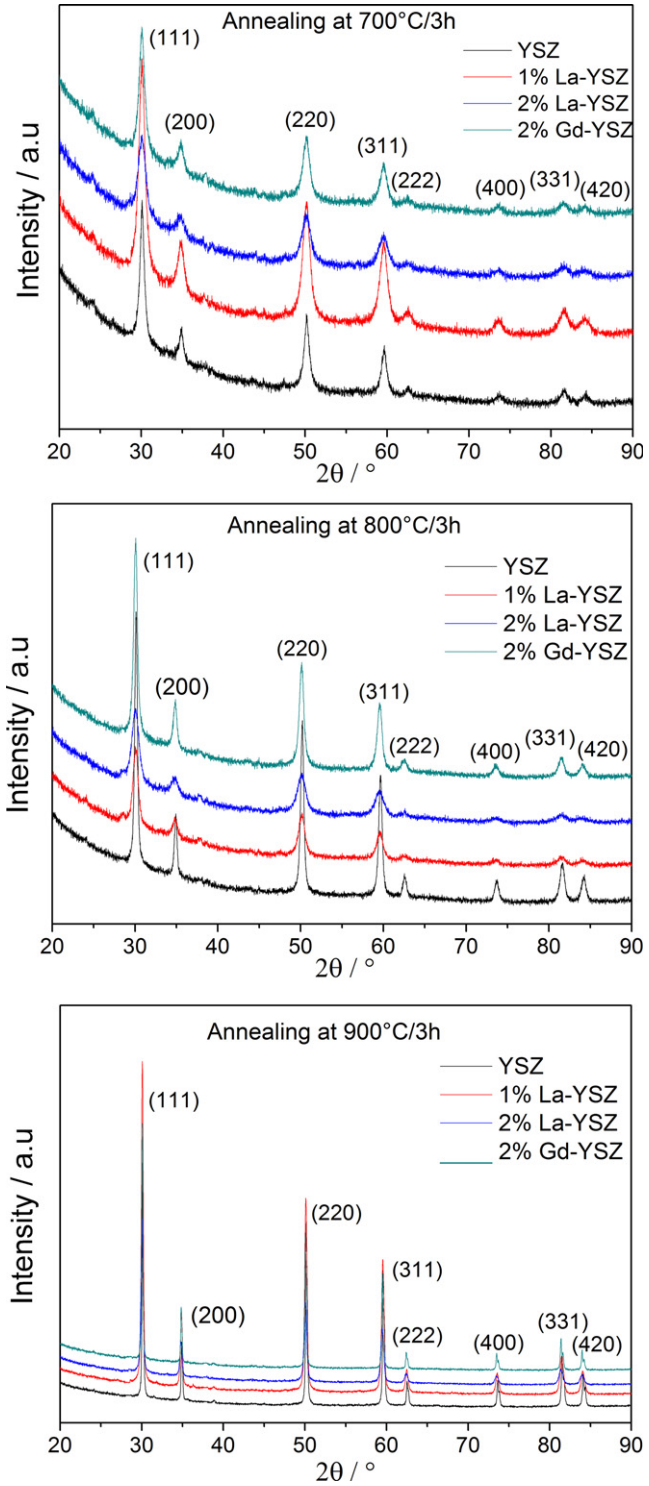

FIGURE 5 XRD patterns of doped and undoped YSZ after annealing. Respective calcination temperatures are indicated in the figure. For all plots, YSZ pattern is the bottom one, followed by 1% La, 2% La and finally 2% Gd at the top

YSZ. Although crystallite growth takes place with annealing temperature as indicated by peak sharpening, no peak shift was observed. The effect of annealing temperature on

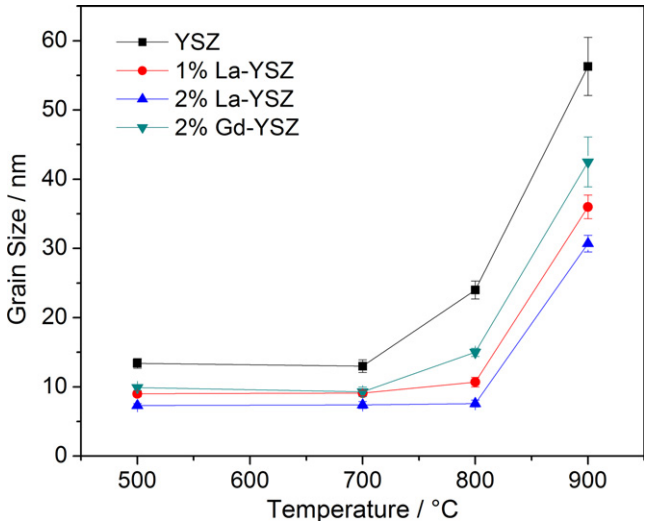

FIGURE 6 Crystallite size of undoped and doped YSZ spheres after annealing. The crystallite size was measured from XRD patterns using Scherer's formula

crystallite size is shown in Figure 6. The dopants were able to stabilize the crystallite size up to 800°C. However, at 900 (and 1000°C, which is not shown as is no longer in the nanometer range, see Figure 7), all the samples showed significant growth, although their final sizes still depended on the dopant type and concentration.

The particle shapes were revealed from the SEM micrographs (Figure 7), where very smooth spherical shapes were observed up to 800°C. Upon further heating, albeit still spherical, the surface of the particles looks slightly porous and rough, with noticeable grains, after 900°C annealing for 3 hours. At 1000°C, the particles resemble the original spheres, but the overall microstructure shows very large grains. The spherical particle sizes from SEM after annealing at different temperatures are plotted in Figure S5 and Figure S2 with the respective size distributions. The particles before calcination show plenty of pores in a vermicular structure. As grains grow, one may suggest that pore coalescence occurs, with pore diameters increasing while keeping the overall volume. This is likely taking place by surface diffusion which is the lowest energy mass transport mechanism and leads to coarsening without densification.

The data in Figure 6 suggest growth continues for all samples regardless of dopant. However, the growth tendency is different for each. For instance, 1% La YSZ shows a slower ramp as compared to 2% La. Still at 900°C, high concentration of La has better growth resistance than 1% La. Interestingly, in the case of 2% Gd YSZ, at 900°C the particles grow more than the La-doped ones. We assume that the re-dissolution of dopant might be responsible for that and cause an increase in grain-boundary energy and result in growth, as suggested in the literature.[43]

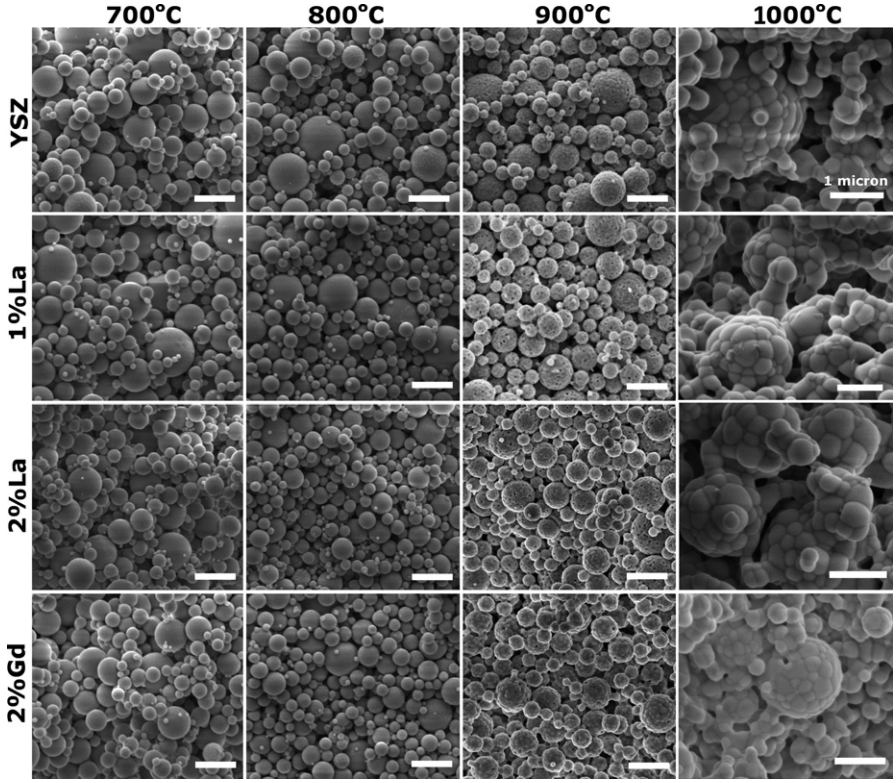

FIGURE 7 SEM micrographs of YSZ and RE-doped YSZ after annealing. The scale bars correspond to 1 micron. The images can be read as in a table, with column and row corresponding to specific composition and temperature. All annealing times are 3 hours

That is, the change in grain-boundary energy as a function of doping can be described by the following equation:

$$\gamma_{gb} = \gamma_0 - \Gamma_B\left(RT\ln X_B^{bulk} - \Delta H_{seg}\right) \quad (1)$$

Here, γ_0 represents the grain-boundary energy of the solvent (host material), Γ_B is the solute excess in the grain-boundary, ΔH_{seg} is the enthalpy of segregation, and X_B^{bulk} is the solute content in the bulk. The equation shows that solute segregation decreases grain-boundary energy and consequently should decrease grain growth by affecting driving force. It has been shown that for Gd-doped YSZ, grain growth can be stopped once a full monolayer of Gd is formed at the grain boundaries.[43] The fraction of monolayer is related to the Γ_B term, which is defined as the solute content per available grain-boundary area. This term is temperature dependent, because the solubility of dopants in the host's structure generally increases with temperature. Therefore, full monolayer coverage is a temperature-dependent function of concentration. For instance, in the system being studied, a geometrical calculation shows that for a grain size at 15 nm, full monolayer coverage of Gd on YSZ requires 8% of Gd when assuming all Gd segregates to the grain boundaries (no solid solution). However, previous work by Nafsin and Castro[43] showed that the solubility of Gd in YSZ increases significantly from 1100°C to 1300°C. It can be calculated from their data that the solubility of Gd in YSZ at 1300°C is around 1.1%. Considering this solubility increase, a total 8% of dopant should only allow full monolayer of Gd if the grain size increases to 40 nm – representing smaller grain-boundary area.

The tested samples so far had only 2% of dopants. This corresponds to about 22% of a monolayer at grain sizes of 15 nm (assuming zero solubility). If a solubility of 1.1 mol % is considered, a grain size of 150 nm is needed to fulfill a monolayer. This is fairly consistent with the observations in Figure 7 that indicates significant grain growth at high temperatures. To further improve stability by targeting a monolayer condition, it is rational to increase the dopant content up to 8%, allowing grain sizes below 40 nm even at high temperatures. However, as will be seen, there were some technical limitations to this approach.

Table 1 shows the results for grain size and particle size for 8% Gd or 8% La YSZ. The data show that the grain size of the USP as-synthesized samples is 15 nm and 9 nm for Gd and La doping, respectively. However, SEM images of the Gd-doped YSZ spheres in Figure 8A reveal very distorted spheres. It is unclear why this happened, but we speculate this is attributed to a change in rheological behavior of the liquid droplets formed during USP due to the high concentrations of Gd ions used in USP, with possible formation of complexes with nitric acid. At the same time, the La-doped samples showed perfect spheres, but a nonnegligible amount of second phase of La_2O_3, as shown in the XRD pattern in Figure S4.

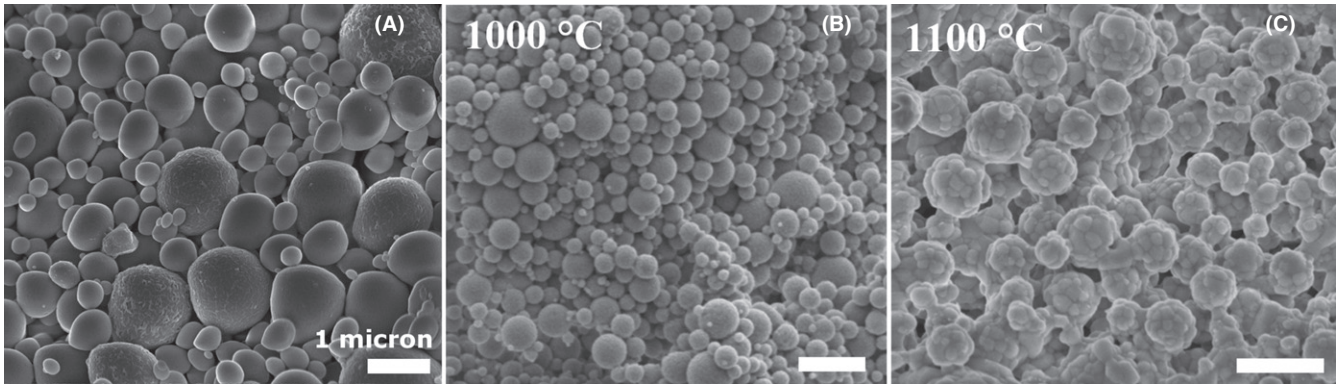

FIGURE 8 A, SEM micrograph of 8%Gd-10YSZ as-synthesized showing nonspherical shapes. B and C, are SEM micrographs of 4%Gd-4% La 10YSZ after annealing. The scale bars correspond to 1 micron. The average particle sizes after 1000°C and 1100°C heating are 336 nm and 344 nm, respectively. Annealing time is 3 hours

The fact that a high concentration of dopant could not provide the anticipated stability benefits without compromising phase or spherical shape invites an alternative approach. To that end, co-doping of the system with Gd and La was explored. The goal was to achieve 8 mol% of dopant while avoiding the shortcoming from having only one component at high concentrations. A 4% La shall not lead to the formation of a second phase, while 4% Gd may have a diluted enough initial solution to avoid rheologial disturbances in the droplets.

USP of YSZ with concentrations 1, 2, and 4% of each doping element (representing a total of 2, 4, and 8% of RE dopants in the system) was performed at 1300°C and the products systematically studied. The produced spheres were highly isotropic and with average particle size of ~300 nm (see Figure S6). From the XRD analyses of all samples, no second phases were observed even for the system with 4% Gd-4% La 10YSZ (Figure S7). Crystallite sizes were measured using whole profile fitting as listed in Table 1, showing a systematic decrease in size as the dopant concentration increased (reaching 8 nm for the 4% Gd- 4% La-YSZ). When compared to the samples with 8 mol% of a single dopant prepared under the same condition (USP at 1300°C), co-doping shows an apparent synergistic effect, not only solving the problems related to the sphere shape and crystallography, but also enabling smaller grain sizes, but the origin of this synergism is still unclear. (Note that one cannot make a direct comparison between the co-doped samples and the single doped ones prepared using USP at 1100°C. Those samples did show smaller grain sizes for the 2 mol% La, but the process is intrinsically different.)

If the mechanisms of stabilization promoted by the single doping are extendable to higher dopant contents, improved thermal stability is attainable for the co-doped systems. To test this hypothesis, the calcined spheres were annealed at 1000°C, 1100°C, and 1200°C for 3 hours and after annealing the samples were analyzed by XRD for phase stability (Figure S8). From the XRD patterns, there was no sign of second phase formation for any of those compositions. Figure 8B,C show the SEM micrographs of 4% Gd-4% La YSZ samples after annealing at different temperatures. Co-dopant clearly retained the spherical shapes of YSZ at higher annealing temperature as compared to single doping. Among the studied compositions, 4 mol% Gd-4 mol% La-YSZ showed best performance, maintaining the spherical shapes after 1100°C annealing. The surface of the particles still looks fairly smooth at 1000°C, signifying less coarsening. Particles after 1000°C annealing retained their spherical shapes without any neck formation. On the other hand, annealing to 1100°C leads to neck formation and grain growth. However, the sphere size remains the same as those from 1000°C heating (~340 nm). The SEM micrographs for higher annealing samples are available in Figure S9.

TABLE 3 Grain size and sphere size of RE-doped YSZ after calcination at 1000°C/3 hours

Sample	BET surface area at 1000°C, m^2/g
1%Gd-1%La YSZ	6.01±0.5
2%Gd-2%La YSZ	13.49±0.7
4%Gd-4%La YSZ	37.76±2.4
8%Gd YSZ	2.87±1.5
8%La YSZ*	3.97±0.4

While maintaining shape and small grain size, relevant for TBC applications, it is important to check the residual porosity after the thermal treatments. In order to know the extent of porosity present in the co-doped YSZ after 1000°C annealing, surface areas were measured using Brunauer-Emmett-Teller (BET) theory. The surface areas are listed in Table 3. The highest surface area was measured for 4%Gd-4%La 10YSZ (~38 m^2/g)

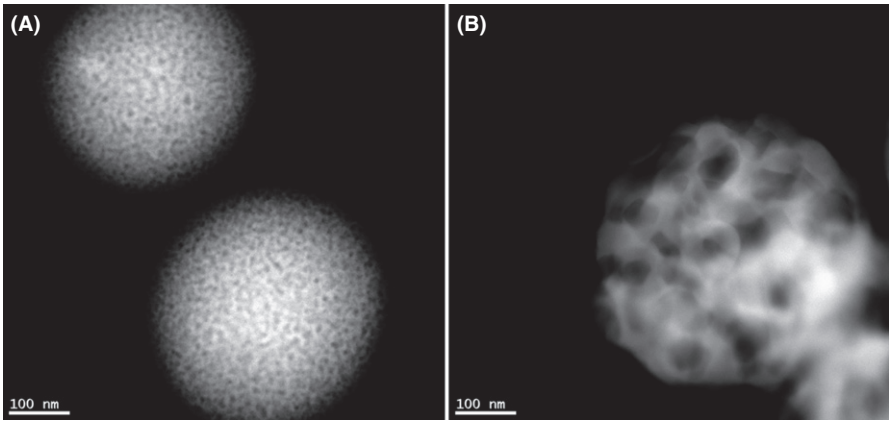

FIGURE 9 STEM micrograph of 4% Gd - 4% La YSZ spheres (A) after calcination at 500°C (B) after annealing 1000°C. The particle (sphere) sizes are 340 nm and 450 nm, respectively

which indicates significant amount of porosity inside the spheres. STEM was also performed on 4%Gd-4%La 10YSZ calcined at 1000°C for 3 hours (Figure 9) and revealed the porous structure. This evidences the role of RE on decreasing grain growth and increasing stability of the spheres.

4 | CONCLUSION

This work demonstrated the possibility of fabricating porous YSZ spherical particles doped with RE using ultrasonic spray pyrolysis. The samples were highly isotropic independent on the composition. RE doping increased thermal stability of the YSZ spherical particles with higher resistance to growth at elevated temperatures as compared to RE-free YSZ. This was likely a result of increased thermodynamic stability (lowering interface energies) as indicated by the DSC results. Although the RE doping increased the stability of YSZ spheres only up to 900°C for 3 hours, co-doping with high concentrations (8%) improved stability up to 1000°C for 3 hours, while at 1100°C the spheres started necking but still retained the spherical shape. These temperatures are, however, still relatively modest if considering turbine applications, but the results shall inspire studies to increase stability using RE. The co-doping seems to be an effective direction to increase stability due to synergistic effects, but further studies are necessary.

ACKNOWLEDGMENTS

This work was supported by the Department of Energy [National Nuclear Security Administration] under Award Number DE-NE0000704 and the German Research Foundation (DFG) via SFB 986 “Tailor-Made Multi-Scale Materials Systems: M3”, project C6.

REFERENCES

1. Cernuschi F, Bianchi P, Leoni M, Scardi P. Thermal diffusivity/microstructure relationship in Y-PSZ thermal barrier coatings. *J Therm Spray Tech*. 1999;8:102-109.
2. DeMasi-Marcin JT, Gupta DK. Protective coatings in the gas turbine engine. *Surf Coat Technol*. 1994;68:1-9.
3. Clarke D, Levi C. Materials design for the next generation thermal barrier coatings. *Annu Rev Amter Res*. 2003;33:383-417.
4. Cao X, Vassen R, Stoever D. Ceramic materials for thermal barrier coatings. *J Eur Ceram Soc*. 2004;24:1-10.
5. Miller RA. Thermal barrier coatings for aircraft engines: history and directions. *J Therm Spray Tech*. 1997;6:35-42.
6. Lee KN, Miller RA, Jacobson NS. New Generation of plasma-sprayed mullite coatings on silicon carbide. *J Am Ceram Soc*. 1995;78:705-710.
7. Chraska P, Dubsky J, Neufuss K, Pisacka J. Alumina-base plasma-sprayed materials part I: phase stability of alumina and alumina-chromia. *J Therm Spray Tech*. 1997;6:320-326.
8. Xu H, Guo H, Liu F, Gong S. Development of gradient thermal barrier coatings and their hot-fatigue behavior. *Surf Coat Technol*. 2000;130:133-139.
9. Brunauer G, Frey F, Boysen H, Schneider H. High temperature thermal expansion of mullite: an in situ neutron diffraction study up to 1600 °C. *J Eur Ceram Soc*. 2001;21:2563-2567.
10. Lima C, Trevisan R. Temperature measurements and adhesion properties of plasma sprayed thermal barrier coatings. *J Therm Spray Tech*. 1999;8:323-327.
11. Tamura M, Takahashi M, Ishii J, Suzuki K, Sato M, Shimomura K. Multilayered thermal barrier coating for land-based gas turbines. *J Therm Spray Tech*. 1999;8:68-72.
12. Slifka A, Filla B, Phelps J, Bancke G, Berndt C. Thermal conductivity of a zirconia thermal barrier coating. *J Therm Spray Tech*. 1998;7:43-46.
13. Bengtsson P, Ericsson T, Wigren J. Thermal shock testing of burner cans coated with a thick thermal barrier coating. *J Therm Spray Tech*. 1998;7:340-348.
14. Di Girolamo G, Blasi C, Schioppa M, Tapfer L. Structure and thermal properties of heat treated plasma sprayed ceria–yttria co-stabilized zirconia coatings. *Ceram Int*. 2010;36:961-968.

15. Vassen R, Cao X, Tietz F, Basu D, Stöver D. Zirconates as new materials for thermal barrier coatings. *J Am Ceram Soc*. 2000;83:2023-2028.
16. Cao X, Vassen R, Tietz F, Stoever D. New double-ceramic-layer thermal barrier coatings based on zirconia–rare earth composite oxides. *J Eur Ceram Soc*. 2006;26:247-251.
17. Ramaswamy P, Seetharamu S, Rao K, Varma K. Thermal shock characteristics of plasma sprayed mullite coatings. *J Therm Spray Tech*. 1998;7:497-504.
18. Thornton J, Majumdar A, McAdam G. Enhanced cerium migration in ceria-stabilised zirconia. *Surf Coat Technol*. 1997;94:112-117.
19. Cao X, Vassen R, Jungen W, Schwartz S, Tietz F, Stöver D. Thermal stability of lanthanum zirconate plasma-sprayed coating. *J Am Ceram Soc*. 2001;84:2086-2090.
20. Kelly MJ, Wolfe DE, Singh J, Eldridge J, Zhu DM, Miller R. Thermal Barrier Coatings Design with Increased Reflectivity and Lower Thermal Conductivity for High-Temperature Turbine Applications. *Int J Appl Ceram Technol*. 2006;3:81-93.
21. Zhu D, Miller RA. Development of advanced low conductivity thermal barrier coatings. *Int J Appl Ceram Technol*. 2004;1:86-94.
22. Leib EW, Vainio U, Pasquarelli RM, et al. Synthesis and thermal stability of zirconia and yttria-stabilized zirconia microspheres. *J Colloid Interface Sci*. 2015;448:582-592.
23. Leib EW, Pasquarelli RM, Blankenburg M, et al. High-temperature stable zirconia particles doped with yttrium, lanthanum, and gadolinium. *Part Part Syst Char*. 2016;33:645-655.
24. Pattanayak A, Subramanian A. Impact of porogens on the pore characteristics of zirconia particles made by polymer-induced colloid aggregation. *Int J Appl Ceram Technol*. 2011;8:94-111.
25. Annen M, Kizhappali R, Carr P, McCormick A. Development of porous zirconia spheres by polymerization-induced colloid aggregation—effect of polymerization rate. *J Mater Sci*. 1994;29:6123-6130.
26. Sun L, Annen MJ, Lorenzano-Porras F, Carr PW, McCormick AV. Synthesis of porous zirconia spheres for HPLC by polymerization-induced colloid aggregation (PICA). *J Colloid Interface Sci*. 1994;163:464-473.
27. Sathyagal A, Carr P, McCormick A. Synthesis of porous zirconia spheres—mechanism and prospects for multistep processing. *J Colloid Interface Sci*. 1999;219:20-30.
28. Yan B, McNeff CV, Chen F, Carr PW, McCormick AV. Control of synthesis conditions to improve zirconia microspheres for ultrafast chromatography. *J Am Ceram Soc*. 2001;84:1721-1727.
29. Yan B, McNeff CV, Carr PW, McCormick AV. Synthesis and characterization of submicron-to-micron scale, monodisperse, spherical, and nonporous zirconia particles. *J Am Ceram Soc*. 2005;88:707-713.
30. Fegley B, Barringer EA. Synthesis, characterization, and processing of monosized ceramic powders. pp. 187 in MRS Proceedings. 2011. Vol. 32.
31. Ogihara T, Mizutani N, Kato M. Processing of monodispersed ZrO_2 powders. *Ceram Int*. 1987;13:35-40.
32. Lerot L, Legrand F, De Bruycker P. Chemical control in precipitation of spherical zirconia particles. *J Mater Sci*. 1991;26:2353-2358.
33. Xia B, Lenggoro IW, Okuyama K. Novel route to nanoparticle synthesis by salt-assisted aerosol decomposition. *Adv Mater*. 2001;13:1579-1582.
34. Chen C, Tseng T, Tsai S, Lin C-K, Lin H. Effect of precursor characteristics on zirconia and ceria particle morphology in spray pyrolysis. *Ceram Int*. 2008;34:409-416.
35. Gaudon M, Djurado E, Menzler NH. Morphology and sintering behaviour of yttria stabilised zirconia (8-YSZ) powders synthesised by spray pyrolysis. *Ceram Int*. 2004;30:2295-2303.
36. Tsai S, Song Y, Tsai C, Yang C, Chiu W, Lin H. Ultrasonic spray pyrolysis for nanoparticles synthesis. *J Mater Sci*. 2004;39:3647-3657.
37. Esparza-Ponce H, Reyes-Rojas A, Antunez-Flores W, Miki-Yoshida M. Synthesis and characterization of spherical calcia stabilized zirconia nano-powders obtained by spray pyrolysis. *Mater Sci Eng, A*. 2003;343:82-88.
38. Okuyama K, Lenggoro IW. Preparation of nanoparticles via spray route. *Chem Eng Sci*. 2003;58:537-547.
39. Messing GL, Zhang SC, Jayanthi GV. Ceramic powder synthesis by spray pyrolysis. *J Am Ceram Soc*. 1993;76:2707-2726.
40. Lenggoro IW, Hata T, Iskandar F, Lunden MM, Okuyama K. An experimental and modeling investigation of particle production by spray pyrolysis using a laminar flow aerosol reactor. *J Mater Res*. 2000;15:733-743.
41. Scott H. Phase relationships in the zirconia-yttria system. *J Mater Sci*. 1975;10:1527-1535.
42. Dey S, Chang C-H, Gong M, Liu F, Castro RHR. Grain growth resistant nanocrystalline zirconia by targeting zero grain boundary energies. *J Mater Res*. 2015;30:2991-3002.
43. Nafsin N, Castro RHR. Direct measurements of quasi-zero grain boundary energies in ceramics. *J Mater Res*. 2017;32:166-173.
44. Castro RHR. On the thermodynamic stability of nanocrystalline ceramics. *Mater Lett*. 2013;96:45-56.
45. Quach DV, Castro RHR. Direct measurement of grain boundary enthalpy of cubic yttria-stabilized zirconia by differential scanning calorimetry. *J Appl Phys*. 2012;112:083527.
46. Chang C-H, Gong M, Dey S, Liu F, Castro RHR. Thermodynamic stability of SnO^2 nanoparticles: the role of interface energies and dopants. *J Phys Chem C*. 2015;119:6389-6397.
47. Yuan F, Chen C, Kelder E, Schoonman J. Preparation of zirconia and yttria-stabilized zirconia (YSZ) fine powders by flame-assisted ultrasonic spray pyrolysis (FAUSP). *Solid State Ionics*. 1998;109:119-123.
48. Zhao H, Yu F, Bennett TD, Wadley HN. Morphology and thermal conductivity of yttria-stabilized zirconia coatings. *Acta Mater*. 2006;54:5195-5207.

SUPPORTING INFORMATION

Additional Supporting Information may be found online in the supporting information tab for this article.

How to cite this article: Nafsin N, Li H, Leib EW, Vossmeyer T, Stroeve P, Castro RHR. Stability of rare-earth-doped spherical yttria-stabilized zirconia. *J Am Ceram Soc*. 2017;00:1–11. https://doi.org/10.1111/jace.14971